Research Article Vol. 30, No. 23 / 7 Nov 2022 / Optics Express 41671
Optics EXPRESS

# Littrow 3D measurement based on 2D grating dual-channel equal-optical path interference

YUNFEI YIN,[1,2] LIN LIU,[1] YU BAI,[1] JIRIGALANTU,[1] HONGZHU YU,[1] BAYANHESHIG,[1] ZHAOWU LIU,[1,*] AND WENHAO LI[1]

[1] *Changchun Institute of Optics, Fine Mechanics and Physics, Chinese Academy of Sciences, Changchun 130033, China*
[2] *University of Chinese Academy of Sciences, Beijing 101408, China*
[*] *zhaowuliu@ciomp.ac.cn*

**Abstract:** We propose a 3D measurement method based on 2D grating dual-channel and Littrow equal-optical path incidence to detect the 3D displacement of a 2D grating in the *X*-, *Y*-, and *Z*-directions. The 2D grating is combined with the Littrow incidence method and a turning element to cause the Littrow diffracted light with frequency $f_1$ to interfere with the reference light at frequency $f_2$, and the displacement data in the *X*-, *Y*-, and *Z*-directions are obtained using the separation-dual-channel phase decoupling algorithm. A corresponding test experimental platform is constructed, and linear error evaluation and step error evaluation experiments are performed to determine the displacements in the *X*-, *Y*-, and *Z*-directions. The results obtained show that all linearity errors are within ±60 nm in the 10 mm measurement ranges in the *X*-, *Y*-, and *Z*-directions, and the test resolution is within ±5 nm. The proposed method can thus realize nanoscale synchronous measurement of *X*-, *Y*-, and *Z*-direction 3D displacements.



## 1. Introduction

Displacement measurement technology is widely used in the fields of ultra-precision machining, optical alignment, and high-precision semiconductor manufacturing [1]. Ultra-precision machining and ultra-accurate positioning [2] can only be achieved when ultra-precision measurement is realized [3]. The most widely used of the existing ultra-precision displacement measurement devices include three-coordinate measuring machines, laser interferometers, and grating rulers. However, increases in the measurement range and measurement dimensions will affect the measurement accuracy of these systems, thus making it necessary to design a displacement measurement system that can realize ultra-high precision and multi-dimensional (multi-D) measurements simultaneously [4]. Currently, many research teams worldwide are attempting to realize ultra-precise multi-D displacement measurements and ultra-accurate information feedback systems to promote the development of ultra-high-precision multi-D displacement measurement technology [5,6]. In the noncontact measurement field, the most common laser measurement method is based on the laser wavelength, has a large measurement range, a simple principle and structure, and can realize multi-D measurements [7]. The grating measurement method is based on the grating pitch, has low sensitivity to the measurement environment, and can achieve high measurement resolution and stability [8]. Currently, the grating measurement method is being developed further to perform ultra-high-precision multi-D displacement measurements based on use of a 2D grating.

In high-precision multi-D displacement measurements based on 2D gratings, multi-D measurement is usually achieved by adding multiple interference units in combination with diffractive units [9], and interference is achieved using tiled 2D transmission gratings or Michelson structures [10] and shear 2D grating or shear laser measurements [11]. Gao's team used a scanning 2D grating and a measuring 2D grating to achieve 3D displacement measurements and used a collimating unit and a four-quadrant position detector design to achieve 3D angle measurements

#475830 https://doi.org/10.1364/OE.475830
Journal © 2022 Received 15 Sep 2022; revised 11 Oct 2022; accepted 13 Oct 2022; published 27 Oct 2022

Optics EXPRESS

based on diffraction interference. These configurations were then combined to achieve 6D high-precision manufacturing [12–14]. Lin's team used a combination of the two-order diffracted light from a 2D grating and phase decoupling under vertical incidence conditions to achieve 2D displacement measurements with a high signal-to-noise ratio and high contrast by using different spatial positions [15]. Zhang's team used the two-order diffracted light from four 1D gratings to construct a high-precision 6D measurement model of real-time lithography scanner displacement [16]. Our team used the 1D grating Littrow incidence method to obtain long-stroke 2D displacement information [17] and obtained ultra-high-precision 2D displacement measurements via Doppler steering interferometry based on vertical incidence on the 2D grating [18]; we also obtained long-stroke high-precision 2D displacement information using a 2D grating and double-spatial heterodyne optical path interleaving [19]. However, 3D measurements based on a 2D grating have the problems of a low *Z*-direction measurement range and low measurement accuracy, and the high-precision multi-D measurement requirements cannot be guaranteed to be met in three dimensions simultaneously. In this paper, we introduce a Littrow 3D measurement method based on 2D grating dual-channel equal-optical path interference that uses turning elements and phase decoupling in combination with 2D grating dual-channel and Littrow equal-optical path incidence to realize displacement measurements of the *X*-grid line, the *Y*-grid line, and the *Z*-normal line at the same time; the following text will describe the proposed method in detail and verify the feasibility of this technique.

## 2. Measurement principle

### 2.1. 2D grating plane displacement measurement theory (X- and Y-directions)

The structure of the proposed 2D grating-based Littrow 3D displacement measurement system is shown in Fig. 1, where the *X*-grid and *Y*-grid lines of the 1200 l/mm 2D grating moving along the positive directions of the stage are taken as the positive directions, the vertical 2D grating plane is in the *Z*-normal direction, and the light is transmitted along the X-grid and *Y*-grid lines direction of the 2D grating, as shown in the front view in Fig. 1(a).

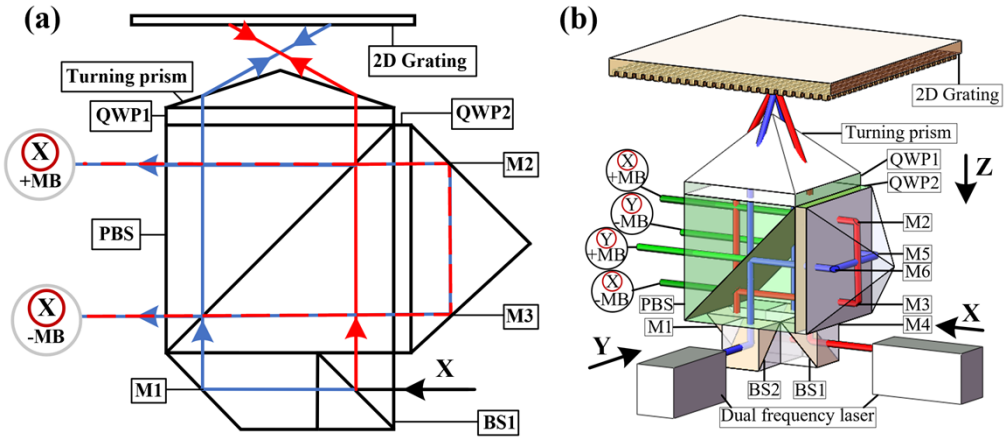


**Fig. 1.** Schematic diagram of the displacement measurement principle based on a 2D grating and a Littrow incident structure. (a) Front view; (b) side view.

The incident light from the dual-frequency laser is split using beam splitters (BS1).

The Measuring beam X-(+MB):

BS1 – PBS (the reflected light (red light)) – QWP1(the transmitted light) – Turning prism – 2D Grating (at the Littrow angle) – Turning prism – QWP1 – PBS (the (+1, 0)-order diffracted light) – X accepts the unit -(+MB).

Optics EXPRESS

BS1 – M1(the transmitted light (blue light)) – PBS – QWP2(the reflected light) – M3 – M2 – QWP2 – PBS (the reference light) – X accepts the unit -(+MB).

The Measuring beam X-(-MB):

BS1 – PBS (the reflected light (red light)) – QWP2(the reflected light) – M2 – M3 – QWP2 – PBS (the reference light) – X accepts the unit -(-MB).

BS1 – M1(the transmitted light (blue light)) – PBS – QWP1(the transmitted light) – Turning prism – 2D Grating (at the Littrow angle) – Turning prism – QWP1 – PBS (the (-1, 0)-order diffracted light) – X accepts the unit -(-MB).

Along the $Y$-grid line direction (blue light) of the 2D grating, as shown in the side view of Fig. 1(b), the following occurs.

The incident light (blue light) from the dual-frequency laser is split by BS2.

The Measuring beam Y-(+MB):

BS2 – PBS (the reflected light) – QWP1(the transmitted light) – Turning prism – 2D Grating (at the Littrow angle) – Turning prism – QWP1 – PBS (the $(0, +1)$-order diffracted light) – Y accepts the unit -(+MB).

BS2 – M4(the transmitted light) – PBS – QWP2(the reflected light) – M5 – M6 – QWP2 – PBS (the reference light) – Y accepts the unit -(+MB).

The Measuring beam Y-(-MB):

BS2 – PBS (the reflected light) – QWP2(the reflected light) – M6 – M5 – QWP2 – PBS (the reference light) – Y accepts the unit -(-MB).

BS2 – M4(the transmitted light) – PBS – QWP1(the transmitted light) – Turning prism – 2D Grating (at the Littrow angle) – Turning prism – QWP1 – PBS (the $(0, -1)$-order diffracted light) – Y accepts the unit -(-MB).

According to the principle of Littrow interferometric measurement, when simultaneously incident on the 2D grating with a diagonal symmetrical distribution, the diagonal diffracted light (the $(+1, 0)$-, $(-1, 0)$-, $(0, +1)$-, and $(0, -1)$-orders of the 2D grating diffracted light) is used, where the following occurs.

In the stationary state, starting from the incidence of the reflected light (the red light) and the transmitted light (the blue light) on the PBS, the first channel (+MB) and the second channel (-MB) have the same optical path difference.

Along the direction of the 2D grating $X$-grid line:

The $(+1, 0)$-order diffracted light with frequency $f_1$ interferes with the reflected light with frequency $f_2$, and the resulting Doppler frequency shift is: $f_1 - f_2 + \Delta f$.

The $(-1, 0)$-order diffracted light with frequency $f_1$ interferes with the reflected light with frequency $f_2$, and the resulting Doppler frequency shift is: $f_1 - f_2 - \Delta f$.

Along the direction of the 2D grating $Y$-grid line:

The $(0, +1)$-order diffracted light with frequency $f_1$ interferes with the reflected light with frequency $f_2$, and the resulting Doppler frequency shift is: $f_1 - f_2 + \Delta f$.

The $(0, -1)$-order diffracted light with frequency $f_1$ interferes with the reflected light with frequency $f_2$, and the resulting Doppler frequency shift is: $f_1 - f_2 - \Delta f$.

Using the phase decoupling method, two opposite displacement signal values are generated along the direction of the 2D grating's $X$-grid line, and subtraction can be obtained at $2\Delta f$; similarly, two opposite displacement signal values will be generated in the $Y$-grid line direction, and by calculating the opposite signals for the two channels, the displacement values $\Delta x$ and $\Delta y$ along the $X$- and $Y$-directions can be calculated.

According to the theory of Doppler frequency shift and displacement transformation [8], the changes in the phase shift can be expressed as follows:

$$\phi_1 = -\frac{2\pi}{\lambda} \cdot \frac{\Delta x}{\sin\theta} \tag{1}$$

Optics EXPRESS

$$\phi_2 = -\frac{2\pi}{\lambda}\frac{\Delta y}{\sin\theta} \tag{2}$$

where $\lambda$ is the incident light wavelength, $\Delta x$ and $\Delta y$ are the displacement changes along the $X$- and $Y$-directions, $k_i$ and $k_t$ are the total distance change coefficients of incident and reflected diffraction interference light under different interference diffraction conditions, respectively, and $\theta$ is the angle between the angle of incidence of the light and the $Z$-axis. According to the 2D grating displacement measurement equation, $n_l \sin\alpha_{mn}\cos\theta_{mn} = \sin\alpha\cos\theta + m\lambda/d_x$ and $n_l \sin\alpha_{mn}\sin\theta_{mn} = \sin\alpha\sin\theta + n\lambda/d_y$, where $n_l$ represents the refractive index in different media, $\theta_{mn}$ is the change in the diffraction angle of the diffracted light, $\alpha_{mn}$ is the azimuthal change in the projection of the diffracted light relative to the grid line direction, and $m$ and $n$ are the diffraction orders along the two grid lines of the 2D grating. Additionally, $\alpha$ are the azimuth angle change of the incident light, and $d_x$ and $d_y$ are the grid line constants of the 2D grating along the $X$- and $Y$-directions, respectively [18,19]. In this paper, the selected 2D grating has $d_x = d_y$; the $X$- and $Y$-direction displacement values obtained can then be fed back through subsequent electrical signal processing.

### 2.2. 2D grating normal displacement measurement theory (Z-direction)

In the measurement system, the light moves away from the reading head along the $Z$-normal direction of the 2D grating. The principle of the test method is shown schematically in Fig. 2. The point at which the difference between the two reference spot positions is half a wavelength is used as the initial zero point, and the phase value of the Doppler frequency shift along the $Z$-direction can then be expressed as:

$$\phi_3 = -\frac{2\pi}{\lambda}\cdot\frac{\Delta x}{\sin\alpha}\cos\theta + \frac{2\pi}{\lambda}\cdot\frac{\Delta z}{\cos\alpha}\cos\theta \tag{3}$$

$$\phi_4 = \frac{2\pi}{\lambda}\cdot\frac{\Delta x}{\sin\alpha}\sin\theta + \frac{2\pi}{\lambda}\cdot\frac{\Delta z}{\cos\alpha}\sin\theta \tag{4}$$

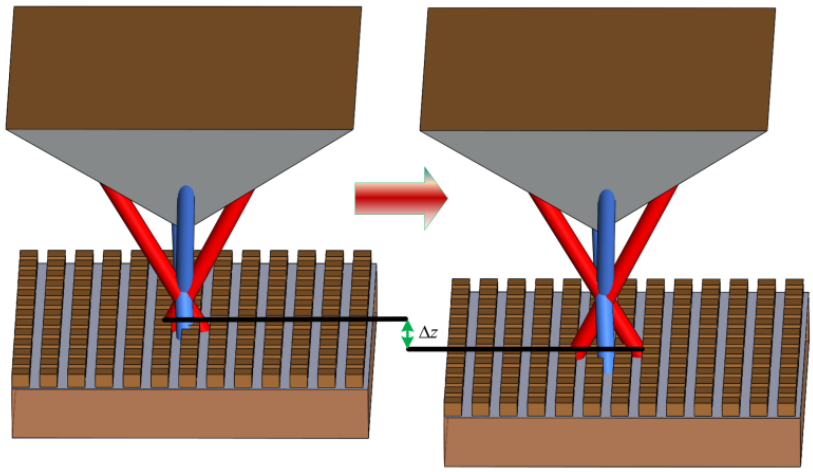


**Fig. 2.** Schematic diagram of Z-direction structure based on 2D grating.

In the above, the displacement of the two beams along the $Z$-normal direction changes as follows:

$$\Delta z = \frac{\lambda\cos\alpha(\phi_4\cos\theta + \phi_3\sin\theta)}{\pi\sin 2\theta(1+\sin\alpha\cos\alpha)} \tag{5}$$

According to the analysis above, there is a fixed π/2 phase difference between the optical signal received at the detector and the displacement in the $Z$-direction, when the displacement in the

Optics EXPRESS

$Z$-direction is $2N$ times the phase difference, the light intensity of the optical signal changes by one cycle, and this one cycle indicates that the phase quantity changes by π.

## 3. Separation-dual-channel phase decoupling algorithm

The 3D experimental data obtained from the measurements are processed as $XYZ$ 3D information, where the $X$- and $Y$-directions are based on the 2D grating pitch, and the $Z$-direction is determined based on the laser wavelength; the information is obtained using dual-channels designated ± MB. First, the integer parts and the decimal parts of the 3D displacement measurement data are extracted; the frequency doubling method is used to extract the integer part that appears, the grating displacement measurement data and the laser displacement measurement data are processed and enlarged to ensure that the phase difference between the two data sets remains stable and unchanged, and the revised signal value is then obtained, where the laser displacement measurement can not only form a 3D contrast with the 2D grating displacement measurement experiment, but also participate in signal processing as a reference signal to form a dual channel ± MB. The dual-channel decoupling method is used to process the extracted decimal's part, which involves the 2D grating displacement measurement data and the laser displacement measurement data of the decimal part of the test doing geometric operations. The phase measurement accuracy is improved within the same frequency value range, and a final stable phase difference value is then obtained.

The measured signal value is divided into several areas, where each area involves the coupling of multiple sine wave signals, and by taking one area as a segment and then performing segmental progressive compensation over the entire area, correction of the 2D displacement measurement signal value can finally be realized. The output phase change curve equation for the selected integer part can then be expressed as follows:

$$\Delta\varphi = N\varphi_1 - N\varphi_2 \tag{6}$$

where $\varphi_1$ and $\varphi_2$ represent the changes in the integer output phase value of the dual-frequency laser interferometer and the 2D grating interferometer, respectively, $N$ is the magnification, and $\Delta\varphi$ is the change in the phase difference value; the coarse change values are then marked, and moderate translation and extended processing is performed on the marked points. When $\Delta\varphi$ remains consistent within a specified range, the integer processing part is then output.

It can be expressed as: the positive and negative measurement signals and the shifting signal are multiplied by analog-to-digital conversion, and after multiplying with the reference signal after low-pass filtering, a stable phase value change is obtained; where, the decimals parts of the dual-frequency laser displacement measurement signal and the 2D grating displacement measurement signal can be expressed as follows:

$$s_1(t) \propto \cos\left[2\pi\frac{f_0}{f_s}t + \varphi\right] \propto \cos(\omega_0\Delta nt + \varphi) \tag{7}$$

$$s_2(t) \propto \cos\left[2\pi\frac{f_0 + \Delta f}{f_s}t + \varphi\right] \propto \cos(\omega_0\Delta nt + \Delta\omega\Delta nt + \varphi) \tag{8}$$

$$s_3(t) \propto \cos\left[2\pi\frac{f_0 - \Delta f}{f_s}t + \varphi\right] \propto \cos(\omega_0\Delta nt - \Delta\omega\Delta nt + \varphi) \tag{9}$$

where $\omega_0 = 2\pi f_0$, $\Delta n = 1/f_s$, $\Delta\omega = 2\pi\Delta f$, $\Delta nt = T_0, T_1, \ldots\ldots T_{M-1}$, ($T_0 = 0$, $T_1 = \Delta n, \ldots\ldots T_{M-1} = (M-1)\ \Delta n$), $\omega_0$ is the initial angular frequency change, $f_0$ is the frequency value of the initial Doppler shift, $\Delta n$ is the change in the sampling frequency period, $f_s$ is the sampling frequency caused by Doppler data acquisition, and $\Delta\omega$ is the Doppler frequency shift. In addition, $\Delta f$ is

Optics EXPRESS

the frequency change value of the Doppler frequency shift, $t$ is the number of samples in the different periods, and $T$ is the cycle time variation completed in a single sampling cycle.

By expanding equations (7)– (9) and performing addition and subtraction processing, the solvable value of $\varphi$ is obtained from:

$$B_1 = \arcsin\left(\frac{s_3(T) - s_2(T)}{2\sin(a+b)}\right) \tag{10}$$

$$B_2 = \arccos\left(\frac{s_3(T) + s_2(T)}{2\cos(a+b)}\right) \tag{11}$$

$$\varphi_1 = \frac{B_1 + B_2}{2} \tag{12}$$

where $B_1$ is the phase change amount for the first receiving channel (+MB) when moving in the $X$-direction of the 2D grating, and $B_2$ is the phase change amount for the second receiving channel (−MB) when moving in the $X$-direction of the 2D grating. According to the principle of least squares, the matrix can be expressed as follows:

$$\begin{cases} x^T x B = x^T a \\ x^T x C = x^T b \end{cases} \tag{13}$$

$$x^T = \begin{vmatrix} \cos(\omega_0 T_0) & \cos(\omega_0 T_1) & \cdots & \cos(\omega_0 T_{M-1}) \\ \sin(\omega_0 T_0) & \sin(\omega_0 T_1) & \cdots & \sin(\omega_0 T_{M-1}) \end{vmatrix}, \quad B = \begin{vmatrix} B_1 \\ B_2 \end{vmatrix} \quad C = \begin{vmatrix} C_1 \\ C_2 \end{vmatrix}$$

$$a = \begin{vmatrix} s_1(T_0) \\ s_1(T_1) \\ \vdots \\ s_1(T_{M-1}) \end{vmatrix}, \quad b = \begin{vmatrix} s_2(T_0) \\ s_2(T_1) \\ \vdots \\ s_2(T_{M-1}) \end{vmatrix} \tag{14}$$

where $C_1 = \cos\Delta\omega T$ and $C_2 = \sin\Delta\omega T$. $C_1$ is the amplitude change of the first receiving channel when moving in the $X$-direction of the 2D grating, and $C_2$ is the amplitude change of the second receiving channel when moving in the $X$-direction of the 2D grating. According to Eqs. (13) and (14):

$$B = (x^T x)^{-1} x^T a \qquad C = (x^T x)^{-1} x^T b \tag{15}$$

Figure 3 shows a diagram of the simulation analysis for the separation-dual-channel phase decoupling algorithm that was designed for the 3D test structure. The initial Doppler shift was set to -π/2 to π/2, the initial phase amount was −π/4, and the Doppler shift change value was in the -π/8 to π/8 range. The sampling frequency of a single cycle was changed by 1/1200, and the number of samples in different periods ranged from 0 to π/8. Figure 3(a) shows, at the initial frequency, the amount of the phase value change accepted by the first channel in the *XYZ* channel within the same sampling period, where the highest phase spectrum value is 1.5 and the lowest is −2.5; after solving, all results are converted into positive images, the phase spectrum ranges up to 3.0, and the change in the phase value accepted by the first channel is $\pm 1.5 \times 10^8$. Figure 3(b) shows, under the same conditions, the amount of the phase value change that the second channel in the *XYZ* channel can accept, and the phase spectrum changes in this case are consistent; after solving, the phase value changes accepted by the second channel are $+2 \times 10^{10}$ and $-3 \times 10^{10}$, and frequency doubling conversion is performed on the phase spectrum, thus ensuring that the phase value change remains stable and constant by amplification processing. As shown in

Optics EXPRESS

Fig. 3(c), by dividing the measured signal value area, the amount of change in each area is given as a correction of a piecewise progressive compensation; the fluctuation range of the correction value remains near zero, and the fluctuation difference is changed to the peak-to-peak change of a sine waveform. As shown in Fig. 3(d), by using the matrix operation of the least squares' method, the amplitude changes between the accepted first channel and the second channel was calculated to obtain the phase value change for the decimal place output within a single sampling period, which was stable around zero, where there is a fan-shaped distribution around it, and the unit amplitude change is 0.00375, the grid change of each interference fringe is 0.8 which is basically the same as the distance between the grid lines of the 2D grating. The results from this operation show that the designed *XYZ* direction separation-dual-channel phase decoupling algorithm can improve the accuracy of the measured phase and allow a stable phase difference value to be obtained.

## 4. Performance testing

### 4.1. Experimental setup

To verify the feasibility of the 3D test system, a dual-frequency laser (model: DH-HN250; wavelength: 632.8 nm; laser power: 2.2 mW; stability: less than 5%) (two beams of linear polarization along the orthogonal direction of the *X*-grid and the *Y*-grid) was used to illuminate a 2D diffraction grating with dimensions of 68 mm × 68 mm and a grating pitch of 833.33 nm. The diffraction efficiency at the Littrow angle of this 2D grating can exceed 40%, the vertical incidence diffraction efficiency can reach 80%. For the *XYZ* directional test, a 1D displacement adjustment test platform (model: XM-S) and an optical platform were used; The entire experimental setup was divided into two separation experiments, as shown in Fig. 4(a), in the *XY* directions, where the light is incident on the 2D grating at the Littrow angle in both the *X*- and *Y*-directions. Among the components shown, the BS was used to split the light, the 2D grating was installed on the 1D displacement adjustment test platform, and the 1D displacement adjustment test platform was then installed on the optical platform. The operation of the test platform was adjusted with respect to the displacement to detect the displacement information accurately in the *X*- and *Y*-directions. In the *Z*-direction, as shown in Fig. 4(b), the light was incident on the 2D grating along the symmetrical Littrow incidence angle of the Z-normal line of the 2D grating, and the *Z*-direction displacement information was detected as the stage moved along the *Z*-normal line. To achieve accurate measurements, the control room temperature was set at 21°C±0.2°C. Among the components used, a dual-frequency laser interferometer (10706B) was selected as the contrast unit acting in the *XYZ* directions; during adjustment, we tried to ensure that the two light spots on the 2D grating surface remained on the same horizontal line. In this experiment, we used the test results from the laser interferometer as the accurate values. Therefore, we regarded the rest of the errors as the error values of the 2D grating displacement measurement; at the same time, simple sealing and space vibration isolation measures were also taken around the equipment to reduce the effects of environmental errors.

### 4.2. X-grid and Y-grid line linearity test results

To verify the effectiveness of the 2D grating displacement measurement system under Littrow incidence conditions, the random errors in the measurement system were reduced via a dual-channel design. The laser interferometer control experiments were designed based on the *X*- and *Y*-grid lines. At the same time, the laser incidence height and the center of the plane mirror were adjusted to ensure that the upper surface of the 2D grating remained horizontal, to reduce the Abbe error, and to ensure high reliability for the test results. The 6UPM01590287 2D stage was controlled by ICS to produce linear displacements of 10 mm along the *X*-grid and *Y*-grid lines of the 2D grating. Figure 5(a) shows the linear measurement error diagram for the Littrow

Optics EXPRESS

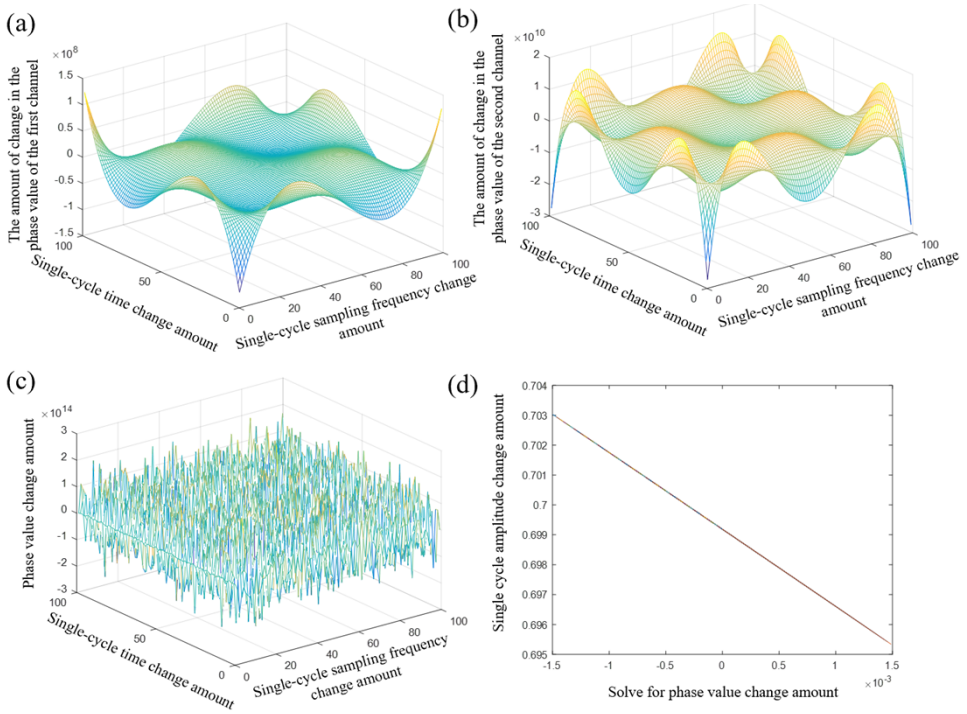


**Fig. 3.** Schematic diagram of the simulation analysis of the separation-dual-channel phase decoupling algorithm.

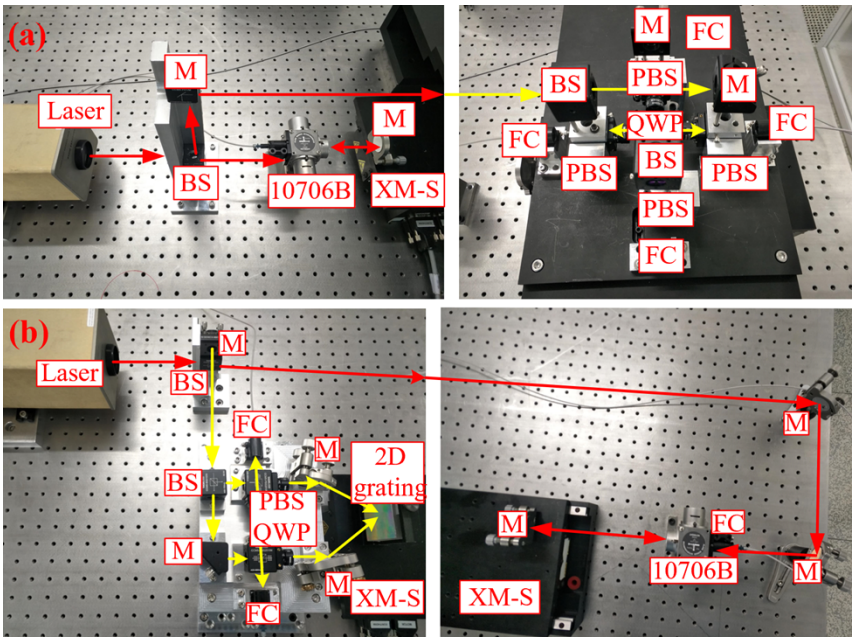


**Fig. 4.** (a) Photographs of the Littrow incidence *XY* grating measurement device; (b) photographs of the Littrow incidence *Z*-normal measurement device.

Optics EXPRESS

incidence X-grid line, where the linear results for the laser measurement and the 2D grating measurement were consistent. Among the results, the measurement error for the 2D grating $X$-grid line 10 mm linear test system was ±60 nm, the maximum two-point jump was ±30 nm, and the minimum two-point jump was ±2 nm. Figure 5(b) is the linear measurement error diagram for the Littrow incidence $Y$-grid line, which shows that the linearity test results were consistent. Among these results, the measurement error for the 2D grating $Y$-grid line test system was ±60 nm, the maximum two-point jump was ±38 nm, and the minimum two-point jump was ±2 nm. Comparison of the measurement results for the $X$-grid and $Y$-grid line displacements of the 2D grating shows that the results obtained using the Littrow incidence method are consistent.

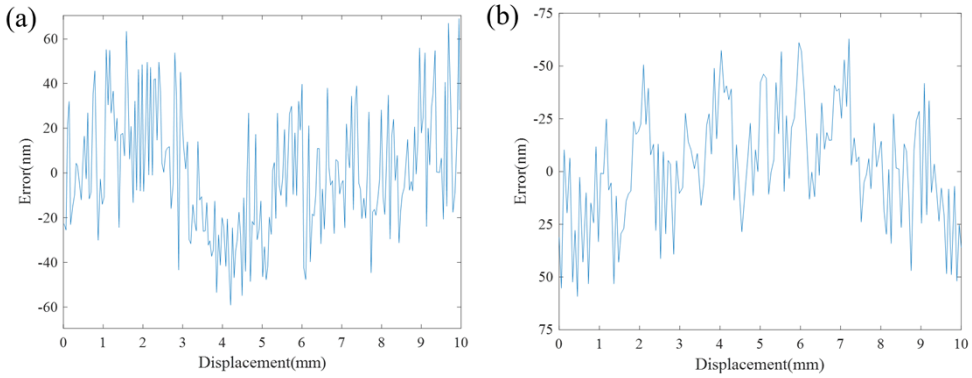


**Fig. 5.** (a) Linear measurement error diagram for the Littrow incidence $X$-grid line; (b) linear measurement error diagram for the Littrow incidence $Y$-grid line.

To verify the displacement measurement accuracy values in the $X$-grid and $Y$-grid directions for the 2D grating in the Littrow incidence mode, the theoretical resolution of the 2D grating displacement measurement system is 0.309 nm. When measured in steps of 10 nm along the $X$-grid and $Y$-grid lines of the 2D grating, as shown in Fig. 6(a), the $3\sigma$ values for the static state of the laser interferometer displacement measurements along the $X$-grid direction and the 2D grating displacement measurements are 2.8456, 3.0453, and 4.4461, and 7.2608, 7.8993, and 8.002, respectively. The corresponding $3\sigma$ values during the movement are 6.0871, 8.1376, and 8.9757, and 9.5610, 11.1787, and 11.4156, respectively. The measurement error fluctuations are ±2 nm and ±4 nm. As shown in Fig. 6(b), for the static state of the laser interferometer displacement measurements along the $Y$-grid direction and the 2D grating displacement measurements, the $3\sigma$ values are 3.3084, 3.8672, and 5.9163, and 8.1640, 8.5538, and 9.0093, respectively. The corresponding $3\sigma$ values during the movement are: 6.6143, 8.0613, and 9.1787, and 10.2081, 10.5485, and 11.9685, respectively. The measurement error fluctuations are again ±2 nm and ±4 nm. The test results show that when compared with the laser interferometers, although the $3\sigma$ fluctuation range and the step error fluctuations for the $X$-grid and $Y$-grid directions of the 2D grating displacement measurement system have reached nanometer-scale precision, the results can also be affected by fluctuations in the measurement environment and the measurement platform; it has been verified experimentally that in the static state, the temperature and the air pressure of the measurement environment are guaranteed to be constant. The airflow crosstalk error that is introduced at the ventilation port can reach ±2 nm, which is consistent with the fluctuations of the laser interferometer that was tested on the workbench. Following multiple adjustments and comparison tests, the measurement platform can introduce an error of ±10 nm without air floatation. These results show that the designed 3D displacement measurement device can realize sufficiently high precision to achieve the intended purpose of nanoscale displacement measurement.

Optics EXPRESS

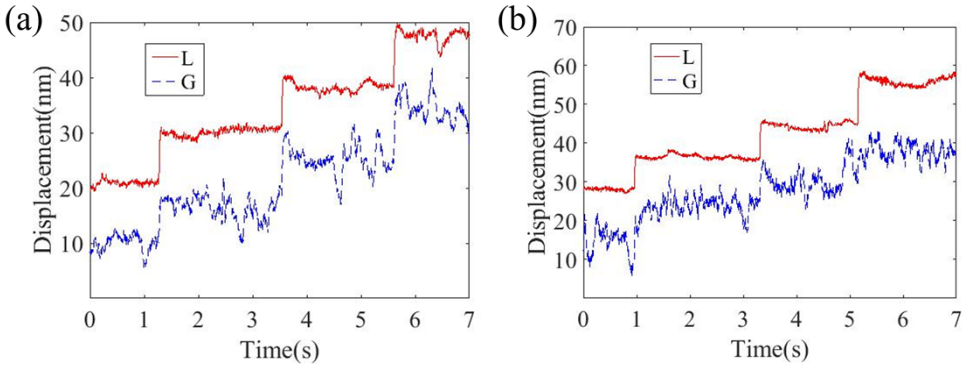


**Fig. 6.** (a) Littrow incidence $X$-grid line nanometer-scale measurement diagram; (b) Littrow incidence $Y$-grid line nanometer-scale measurement diagram.

### 4.3. *Z-normal linearity test results*

To realize displacement measurement of the $Z$-normal, the XM-S model 1D air-floating vibration isolation platform was used to control the displacement stage and move it to the position at which the two incident light spots overlapped. However, following consideration of the influence of the reflected light from the Littrow incidence, the difference between the spot distances was found to be 50% of the spot size. The 2D grating displacement measurement system performed measurements along the Z-normal using the laser wavelength as a benchmark. The theoretical resolution of the measurement system is 0.309 nm. The result of each measurement is the change in the optical path length along the Littrow incidence direction; therefore, the actual measured $Z$-direction distance should be multiplied by a factor of 1.081. The XM-S moves by 10 mm with the 2D grating, and because of the Littrow incidence, there is no ideal parallel and perpendicular state between the 2D grating and the read head, and there is also a specific angular offset $\gamma$. Therefore, it is necessary to determine the amount of change that occurs in the measured Z-normal angle $\gamma$ value within the 10 mm range. Figure 7 shows the test plot for the verticality of the Littrow incidence $Z$-normal, and under the combined influence of the

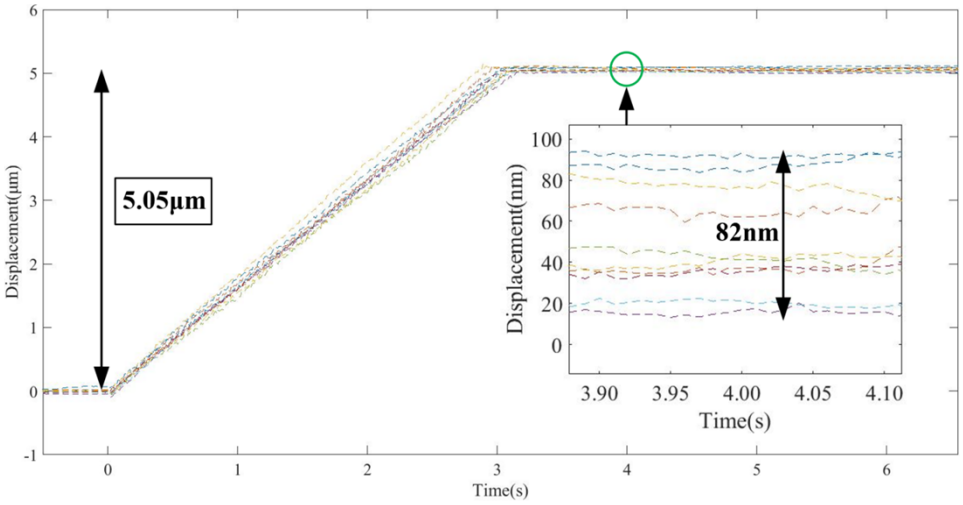


**Fig. 7.** Test plot of the verticality of the Littrow incidence Z-normal.

Optics EXPRESS

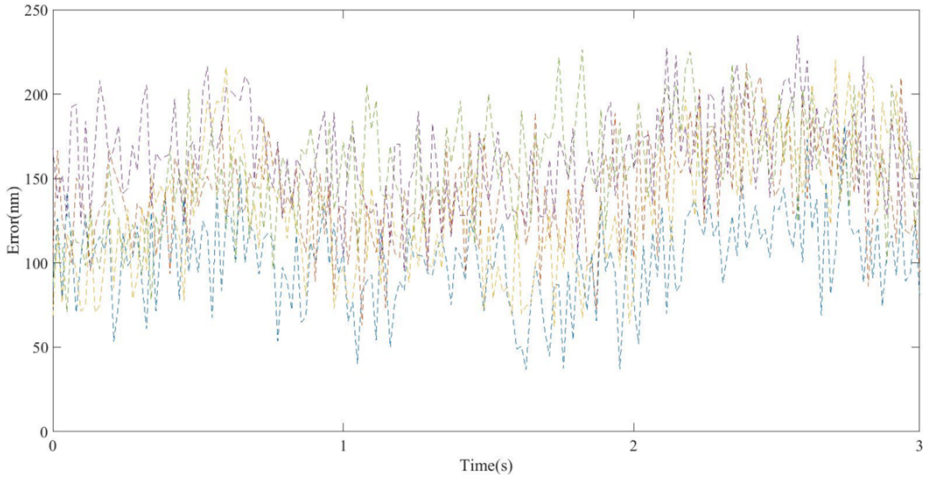


**Fig. 8.** Test results for the verticality error of the Littrow incidence Z-normal.

stage error and the 2D grating error, the yaw change in the measured value is not a regular linear change. According to the measured results, where the measurements were repeated 10 times, the test distance is 10 mm, the measured angle change is: ± 20.2 μrad, and the average value of the verticality change is 5.05 μm; the beating of the linear change amount at the same test point can reach approximately 82 nm, and the minimum beating can reach approximately 2 nm. When fitted using the verticality change value of 5.05 μm, the error value jump is negligible, and at the start and end points, the jump averages for the 2D grating displacement measurement systems are 34 nm and 19 nm, respectively. Therefore, it is necessary to ensure the stability of both the speed and the fluctuations of the device during initial operations before testing.

During the test, we used a symmetrical structure design to ensure that the distances traveled by the two light spots were equal, but one spot traveled in the positive direction and the other traveled in the negative direction. By adding and subtracting the acquired signals and then fitting the test results, the results in Fig. 8 show that in the linear symmetrical test, the test error was maintained at ±75 nm, which can greatly reduce the influence of both environmental errors and 2D grating line errors.

Figure 9 shows the linear measurement results for the Littrow incidence *Z*-normal. The laser interferometer control group experiment was set up along the *Z*-normal direction, thus also ensuring that the laser incidence height, the center of the plane mirror, and the upper surface of the 2D grating all remained highly consistent, and the influence of the Abbe error was also reduced as far as possible. Obviously, within the test range of 10 mm, the test results for the 2D grating displacement measurement system (blue, dotted line) and the laser interferometer test system (red, solid line) remain consistent. The settings of the 2D grating displacement measurement system were not limited by speed and acceleration, and the maximum speed can reach 300 mm/s, while the minimum can be as low as 1 nm/s, but following consideration of the influence of the fluctuation error, the speed was limited to 12 mm/s. Based on the measurement results and the Littrow test angle of 22.314° used to measure the *Z*-normal linear displacement value, the linear displacement of the laser displacement measurement was 9.999777 mm, and the difference between the results from the 2D grating displacement measurement system and those from the laser interferometer was 13.465 nm. Figure 10(a) presents a graph that shows the variation in the *Z*-normal error of the 2D grating displacement measurement, where the error of the 2D grating displacement measurement system was ±60 nm. The maximum measurement distance between the 2D grating displacement measurement system and the laser interferometer

Optics EXPRESS

is 173.52 mm, the minimum is 93.52 mm, and at the test step size of 123.52 mm, the Abbe error introduced is 5.597 μm; the deviation angle between the two devices is ±22.25 μrad, and the deviation angle between the two linearities is ±16.99 μrad. Figure 10(b) shows a graph of the 10 nm step changes in the *Z*-normal line from the 2D grating displacement measurements. The error fluctuation between the laser interferometer and the 2D grating displacement measurement system was ±3 nm, and the $3\sigma$ values for the laser interferometer displacement measurements and the 2D grating displacement measurements during the movement were 4.6831, 8.1376, and 8.9757, and 4.9674, 8.9675, and 9.4023, respectively; the corresponding $3\sigma$ values for the laser interferometer displacement measurements and the 2D grating displacement measurements during the stationary period were 3.0892, 3.4506, and 4.6760, and 3.7202, 4.0359, and 4.8675, respectively. Although the basis of the *Z*-normal test is a 2D grating, this element is essentially equivalent to a mirror; the fundamental reason for the difference is the fluctuations from the signal demodulation process and the environment, while the influence of the Abbe error can be reduced by measuring the linearity of the Abbe error and the fitting method. The *Z*-normal linear measurement stroke of the proposed 3D measurement system can be increased by increasing the range of the 2D grating, which will then allow it to realize nanometer-scale displacement measurements.

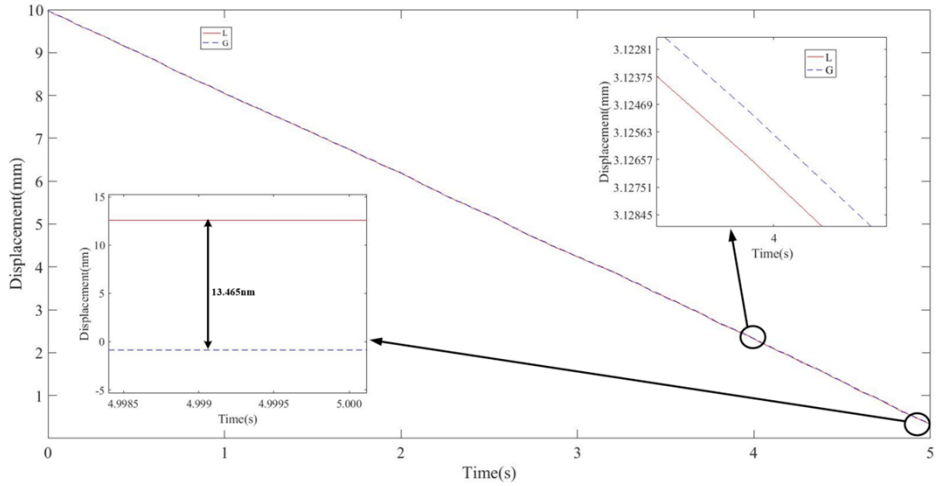


**Fig. 9.** Linear measurement diagram of Littrow incidence Z-normal.

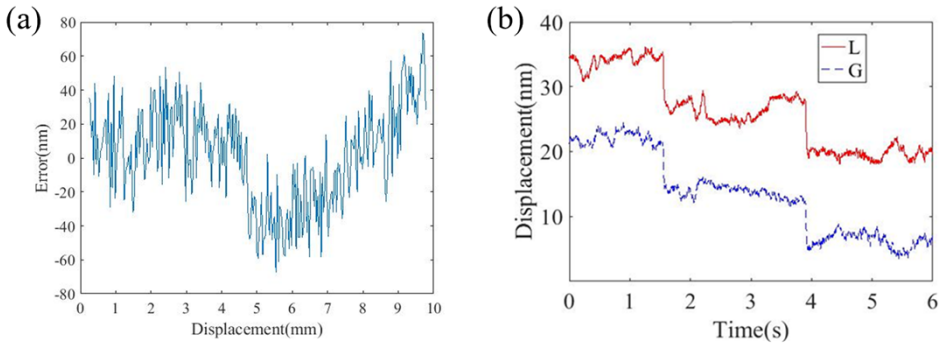


**Fig. 10.** Z-normal measurement diagrams of 2D grating displacement measurement. (a) *Z*-normal linearity error result graph; (b) 10 nm step diagram of the *Z*-normal.

Optics EXPRESS

## 5. Conclusion

The paper proposes a 3D displacement measurement device based on a 2D grating dual-channel and Littrow equal-optical path incidence-type setup that is used to detect the displacement data for the $X$-grid and $Y$-grid lines and the $Z$-normal of the 2D grating. The $X$-grid and $Y$-grid line directions use a design method that combines the dual-channel structure with the Littrow structure. The (1, 0)- and (0, 1)-order diffracted light beams and the (−1, 0)- and (0, −1)-order diffracted light beams with frequency $f_1$ are emitted along the symmetrical Littrow angle and interfere with the reference light beams of (−1, 0)- and (0, −1)-order diffracted light and (1, 0)- and (0, 1)-order incident light with frequency $f_2$. The $Z$-normal direction uses a combination of a symmetrical distribution and the Littrow structure, the interference method is consistent with the $X$-grid and $Y$-grid lines, and the $Z$-normal displacement data are obtained through an angle change of 22.3138°. In this paper, through linear displacement measurements of the $X$-grid and $Y$-grid lines and the $Z$-normal line, and by detection of the measurement system accuracy, the test results show that when measured in the 3D directions of the proposed 2D grating displacement measurement system, the measurement error within a 10 mm range can reach ±60 nm, the test resolution can reach ±5 nm, and the test system fluctuations can be stabilized at ±17 nm. The 3D displacement measurement system designed in this paper can not only realize 2D measurement of the 2D grating-grid line but also can realize $Z$-normal displacement measurement of the long stroke. At the same time, the symmetries of the optical path and the equal-optical path are used to reduce the periodic nonlinear error of the measurement system. In future work, we intend to use multiple 2D gratings and multiple read head structures to achieve 6D measurements and engineering designs.

**Funding.** Changchun Science & Technology Development Program Project in China (21QC03); Strategic Priority Research Program of the Chinese Academy of Sciences (XDC04000000); National Natural Science Foundation of China (62075216, U21A20509).

**Acknowledgments.** This work was supported by the National Natural Science Foundation of China [grant numbers U21A20509, 62075216]; the Strategic Priority Research Program of the Chinese Academy of Sciences [grant number XDC04000000]; the Changchun Science & Technology Development Program Project in China [grant number 21QC03].

**Disclosures.** The authors declare no conflicts of interest.

**Data availability.** Data underlying the results presented in this paper are not publicly available at this time but may be obtained from the authors upon reasonable request.

**Supplemental document.** See Supplement 1 for supporting content.

## References

1. J. D. Ellis, "*Field Guide to Displacement Measuring Interferometry*," M. Bellingham, SPIE: UK, (2014).
2. S. Hasegawa, M. Fujimoto, T. Atsumi, and Y. Hayasaki, "In-process monitoring in laser grooving with line-shaped femtosecond pulses using optical coherence tomography," Light: Adv. Manuf. **3**, 1 (2022).
3. Z. C. Geng, Z. Tong, and X. Q. Jiang, "Review of geometric error measurement and compensation techniques of ultra-precision machine tools," Light: Adv. Manuf. **2**(2), 211–227 (2021).
4. P. C. Hu, D. Chang, J. B. Tan, R. T. Yang, H. X. Yang, and H. J. Fu, "Displacement measuring grating interferometer: a review*," Front. Inf. Technol. Electron. Eng. **20**(5), 631–654 (2019).
5. J. L. Deng, X. N. Yan, C. L. Wei, Y. C. Lu, M. K. Li, X. S. Xiang, W. Jia, and C. H. Zhou, "Eightfold optical encoder with high-density grating," J. Appl. Opt. **57**(10), 2366–2375 (2018).
6. T. Castenmiller, V. D. M. Frank, D. K. Toine, V. D. V. Coen, D. W. Marten, S. Raf, and V. C. Stefan, "Towards ultimate optical lithography with NXT: 1950i dual stage immersion platform," Proc. SPIE **76401N**, 76401N (2010).
7. Y. Hori, S. Gonda, Y. Bitou, A. Watanabe, and K. Nakamura, "Periodic error evaluation system for linear encoders using a homodyne laser interferometer with 10 picometer uncertainty," J. Precis. Eng. **51**, 388–392 (2018).
8. Y. C. Lu, C. L. Wei, W. Jia, S. B. Li, J. J. Yu, M. K. Li, C. X. Xiang, X. S. Xiang, J. Wang, J. Y. Ma, and C. H. Zhou, "Two-degree-freedom displacement measurement based on a short period grating in symmetric Littrow configuration," J. Opt. Commun. **380**, 382–386 (2016).
9. H. L. Hsieh and S. W. Pan, "Development of a grating-based interferometer for six-degree-of-freedom displacement and angle measurements," J. Opt. Express **23**(3), 2451–2465 (2015).
10. H. L. Hsieh and W. Chen, "Heterodyne Wollaston laser encoder for measurement for in-plane displacement," Opt. Express **24**(8), 8693 (2016).

Optics EXPRESS


11. R. Sirohi, "Shearography and its applications – a chronological review," Light: Adv. Manuf. **2**(4), 1 (2021).
12. A. Kimura, W. Gao, W. J. Kim, K. Hosono, Y. Shimizu, L. Shi, and L. J. Zeng, "A sub-nanometric three-axis surface encoder with short-period planar gratings for stage motion measurement," J. Precis. Eng. **36**(4), 576–585 (2012).
13. X. H. Li, W. Gao, H. Muto, Y. Shimizu, S. Ito, and S. Y. Dian, "A six-degree-of-freedom surface encoder for precision positioning of a planar motion stage," Precis. Eng. **37**(3), 771–781 (2013).
14. W. Gao, S. W. Kim, H. Bosse, H. Haitjema, Y. L. Chen, X. D. Lu, W. Knapp, A. Weckenmann, W. T. Estler, and H. Kunzmann, "Measurement technologies for precision positioning," CIRP Ann. **64**(2), 773–796 (2015).
15. C. B. Lin, S. H. Yan, D. Ding, and G. C. Wang, "Two-dimensional diagonal-based heterodyne grating interferometer with enhanced signal-to-noise ratio and optical subdivision," Opt. Eng. **57**(06), 1 (2018).
16. W. T. Zhang, Y. L. Wang, D. Hao, Q. L. Zeng, and X. M. Xiong, "High-precision displacement measurement model for the grating interferometer system," Opt. Eng. **59**(04), 1 (2020).
17. Q. Lv, Z. W. Liu, W. Wang, X. T. Li, S. Li, Y. Song, H. Z. Yu, B. A. Y. A. N. H. E. S. H. I. G. and W, and H. Li, "Simple and compact grating-based heterodyne interferometer with the Littrow configuration for high-accuracy and long-range measurement of two-dimensional displacement," Appl. Opt. **57**(31), 9455–9463 (2018).
18. Y. F. Yin, Z. W. Liu, S. Jiang, W. Wang, H. Z. Yu, W. H. Li, and Jirigalantu, "Grating-based 2D displacement measurement with quadruple optical subdivision of a single incident beam," Opt. Express **29**(15), 24169–24181 (2021).
19. Y. F. Yin, Z. W. Liu, S. Jiang, W. Wang, H. Z. Yu, Jirigalantu, Q. Hao, and W. H. Li, "High-precision 2D grating displacement measurement system based on double-spatial heterodyne optical path interleaving," Opt. Lasers Eng. **158**, 107167 (2022).